Two modes of screw dislocation glide in fcc single-phase concentrated alloys

Yuri N. Osetsky[1]*, *George M. Pharr*[2] *and James R. Morris,* [1,3]

[1] Materials Science and Technology Division, Oak Ridge National Laboratory, Oak Ridge, TN 37831- 6138, USA

[2] Department of Materials Science and Engineeeing, Texas A&M University, College Station, TX 77845-3003

[3]Materials Science and Engineering Department, University of Tennessee, Knoxville, TN 37996

Abstract

Concentrated solid solution alloys (CSSAs), including medium- and high- entropy alloys, are currently being considered as prospective materials in many applications. The behavior of CSSAs under different conditions, including mechanical loading, differs from that of conventional alloys and has been the subject of intensive study by different techniques. In many cases, their behavior is treated by modifying solid solution hardening models, which, in principle, does not reflect many important features of CSSAs where the distinction between solute and solvent atoms is not clear. In this work, we report the results of an atomic-scale study of ½<110>{111} screw dislocation motion in an fcc equiatomic Ni-Fe alloy. Molecular dynamics simulations demonstrate that the dislocation has two distinctive modes for glide. At lower stress, dislocations move in a very rough manner that cannot be described as continuous glide but rather as jerky motion through a set of obstacles. At high stress, they glide in a manner similar to lattice friction-controlled conditions in single component systems. The stress for the transition between modes depends on the dislocation segment length and temperature. At 300K, the flow stress saturates at ~130 MPa for lengths above ~140 $|\boldsymbol{b}|$ ($\boldsymbol{b}$ is the Burgers vector).

---

*Corresponding author e-mail address: osetskiyyn@ornl.gov (Y.N. Osetsky).

1. Introduction

Considerable interest has developed in recent years in understanding the mechanical behavior and properties of concentrated solid solution alloys (CSSAs), including medium- and high- entropy alloys (MEAs and HEAs), i.e., metallic alloys containing approximately equal concentrations of the constituent alloying elements [1-14]. Much of the interest is due to the observation that some of these alloys exist as single-phase, random solid solutions in simple crystalline arrangements [2-4]. It is assumed that the large entropy of mixing produced by the equiatomic proportions can contribute to stabilizing the single-phase structure [5,6]; however, the enthalpy also appears to play an important role [7]. Important examples of such CSSAs are Ni-based single phase face centered cubic structure (fcc) solid solutions, for example, equiatomic FeNiCoCrMn, NiCoCr, NiCoCrMn and FeNiCoCr. Some of these alloys exhibit unique and potentially attractive mechanical properties [1,8-10], including high strength and ductility, with unusual temperature-dependent properties.

An important experimental observation is that dislocation motion in the FCC equiatomic alloys is very sluggish, even at room temperature, suggesting that there is high lattice friction. This was first reported in a TEM study of deformation microstructures in equiatomic FeNiCoCrMn [13]. These investigators observed very planar arrays of relatively straight dislocations slipping on the usual {111} <110> FCC slip systems, which when piled up against grain boundaries, retained very tight spacings, even after unloading, presumably due to a high lattice resistance. Zhang *et al* [14] have used in situ TEM straining techniques to directly observe the dislocation processes that produce deformation in the vicinity of a propagating crack tip in FeNiCoCrMn. As in the other studies, they report high friction stresses and extremely low velocities for the motion of planar arrays of perfect dislocations. However, they also observed that the first dislocations to form are partial dislocations that move very rapidly until their motion is impeded by the formation of planar arrays of more sluggish perfect dislocations. What makes

these observations especially unusual is that in pure FCC metals, lattice friction is usually very low, with dislocation mobility limited primarily by phonon drag processes [15]. On the other hand, in pure BCC metals, lattice friction is much higher due to a greater Peierl's barrier [16,17]. This can contribute significantly to the overall strength of the material, especially at low temperatures, producing a much stronger temperature dependence of the strength. In this sense, the mechanisms of dislocation-based plasticity in FCC equiatomic alloys appear to be more BCC-like than FCC-like.

There have been some efforts to develop theoretical models for dislocation related plasticity of CSSAs. One important recent model is based on the solute strengthening theory [18,19]. A general formalism of solute strengthening was developed for dilute alloys where solutes, taken as "internal obstacles" to the dislocation glide, and their interaction with dislocations can be treated individually. Application of this formalism to edge dislocations in concentrated multicomponent alloys in [19] has demonstrated qualitative and quantitative agreement with experimental observations. However, because of the unknown nature of the internal obstacles, model parameteriazation is rather complicated, and atomic scale modeling both *ab initio* and classical can be used to clarify the details. Unfortunately. *ab initio* methods are not easy to implement in fcc alloys because of the scales needed to capture the behavior of dissociated dislocations. However, classic molecular dynamincs modeling can be quite useful if adequate interatomic potentials are known. To this end, the structure and motion of edge and 60^o dislocations under applied shear stress in FCC alloys have recently been studied using MD methods [20-23]. In addition, recent work on MD modeling of edge dislocations in the equiatomic Ni-Fe alloy using different interatomic potentials over a wide range of applied shear stress [24] has demonstrated sluggish motion relative to pure fcc Ni. The dislocation velocity in this alloy is lower than in Ni, with the effect depending on temperature and the interatomic potentials. However, a basic understanding of CSSAs

during deformation is still rather obscure, and the basic mechanisms responsible for dislocation behavior in concentrated alloys are not at all clear.

In this paper, we report two modes of motion of a screw dislocation in equiatomic Ni-Fe alloy, in comparison with the behavior in pure Ni. We demonstrate that at low stresses, dislocations move in a very discontinuous way, in an obstacle-controlled regime. In contrast, at high stresses, dislocation glide is continuous and smooth, similar to that of pure Ni. Correspondingly, the apparent friction properties of dislocation motion change significantly, and all of these effects depend on the dislocation segment length and temperature. The effects of dislocation length are significant, indicating strong pinning effects, yet the dislocations do not exhibit significant bowing out as would be expected for localized obstacles. In the simulations presented below, the strongest pinning of the dislocations often occur only after dislocation glide of 100 nm or more, suggesting that local configurations along the dislocation line may lead to much stronger pinning than expected for the collective behavior of many solute atoms.

2. The Model

The general description of atomic-scale modeling using a periodic array of dislocations (PADs) can be found elsewhere [25, 26], and the details of screw dislocation construction in an fcc structure are described in [25, 26]. PADs allows for the simulation of the long-range motion of dislocations [24]. This is particularly important in the case of CSSAs, where the statistics of different positions of the dislocation line over the alloy bulk is crucially important for determining dislocation properties under conditions of high chemical disorder. In this case, the properties of gliding dislocation, e.g., the shear flow stress, τ_F, depend on how many positions are visited by the dislocation. Using PADs provides an ideal tool to provide a large number of non-equivalent dislocation positions from a single random alloy configuration.

The simulation cells for the PADs for the present work are the following:

- The crystal size along the ***x***=<110> direction, i.e., along the dislocation line length, is chosen to be in the range of L_D = 4-282 |***b***|, where ***b***= a/2<110> is the dislocation Burgers vector. As demonstrated below, for short values of L_D, the dislocation behavior can vary significantly.
- The crystal size along the dislocation glide direction, ***y***= <112>, is L_y= 70.43a_0, where a_0 is lattice parameter of either pure Ni, which varies from 0.3500 nm to 0.3534 nm or Ni-Fe equiatomic alloy, which varies from 0.3489 nm to 0.3521 nm, over the temperature range 0-900K;
- The crystal size in the direction perpendicular to slip plane, ***z***= <111>, is L_z=35 a_0.

Dislocation motion in PADs follows the Orowan relationship:

$$\varepsilon = \bar{Y} b \rho_D = \bar{Y} \frac{b}{L_y L_z} \text{ , \#(1)}$$

where ε is the plastic strain (here along the <112> direction), and $\bar{Y}$ is the distance of dislocation glide. In PADs, when the total displacement of upper crystal layer (Z>*H*) relative to the lower crystal layer (*Z<0*), equals to *b*=|***b***|, the screw dislocation has moved over the whole crystal in the Y direction, i.e., $\bar{Y} = L_y$ (see [24] for details). This deformation produces one Burgers vector ***b*** slip of the upper half-crystal relatively the lower half-crystal and therefore provides a new configuration for the whole model system, i.e., the local atomic configurations encountered by the dislocation are different due to the slip. The maximum number of such new local atomic configurations is equal to the number of possible such slips (i.e., integral multiples of the Burgers vector ***b***), which in turn equals to L_D/b. Therefore, the longest distance simulated in the same crystal is $\bar{Y}_{max} = L_D L_y / b$ which varies from ~98 nm to ~6900 nm for L_D from 4*b* to 284*b* for the above PADs parameters. Most of modeling here was done for "short", "medium" and "long" dislocations with lengths L_D= *4b*, *64b* and *142b*, respectively, corresponding to $\bar{Y}_{max} \approx$ 98 nm, 1570 nm

and 3500 nm modelled in the same crystal. In practice, we model the motion of dislocations over ~100-800 nm, that is about 300–2400 independent Peierls valleys along the a/2<112> glide direction.

Two deformation modes were used to activate dislocation glide: *stress controlled* and *strain controlled*. In the stress-controlled mode, a constant stress is applied, and the dislocation velocity, v_D, is estimated as the slope of distance-time dependence during steady state glide (see [24]). We utilize this mode to examine the temperature-dependent relationship between stress and dislocation velocity. The applied shear stress, τ, was varied from 5 MPa to 500 MPa, resulting in dislocation steady state velocities, V_D, from ~6 to 400 m/s. This mode is sometimes used to estimate the flow stress, by incrementally increasing the stress before the dislocation starts moving [17]. However, this approach does not allow an accurate estimation of the flow stress for several reasons. First, increasing the stress by a small increment (necessary for accurate estimation) and waiting for a sufficiently long time at each stress increment, demands very large computer resources to produce an accurate result. Second, at high stresses, inertial effects may be significant. This effect may result in an underestimation of the flow stress, especially at low simulated dislocation densities when the effective "inertial" dislocation mass is large. The difficulty of this approach for estimating flow stress will be demonstrated below.

Dislocation glide under strain loading in the alloy is rather different than glide under applied shear stress. Due to the limitations of stress-controlled glide, we therefore applied the strain-controlled mode to estimate the flow stress and to investigate the stress influences on long range dislocation glide. The strain rate, $\dot{\varepsilon}$, was varied from 10^5 $s^{-1}$to 10^8 s^{-1}, equivalent to a dislocation velocity of V_D =0.12-120 m/s.

We have modeled a screw dislocation with the Burgers vector $\boldsymbol{b}$=a/2<110> that, during relaxation, dissociates into Shockley partial dislocations according to the reaction:

$$\mathrm{a}/2 < 110 > = \ a/6 < 21\bar{1} > \ + a/6 < 121 > . \#(2)$$

The partials are separated by an intrinsic stacking fault in a {111} plane. We also examined dislocation line-length effects from L_D = 4|***b***| (~0.99 nm) to 284|***b***| (~70 nm), and find significant effects as detailed below. Dislocation glide was modelled over a wide range of temperature from 10 to 900 K. Temperature was controlled by Berendsen thermostat [28] that is simple and efficient in large systems.

To model interatomic interactions in the Ni-Fe equiatomic alloy, we have used a set of interatomic potentials from [29] created specially to study plasticity in fcc Fe-Ni-Cr alloys. These potentials reproduce the main dislocation properties and stacking faults in these materials. Comparison is made to the behavior of pure Ni.

3. Simulation Results

The ½<110> screw dislocation in pure Ni is highly mobile, as demonstrated in Fig.1 for a dislocation gliding under several applied shear stresses at 300K. The glide distance is a linear function of time at all applied stresses, and the dislocation glide velocity is the slope of this function. Results in pure Ni do not depend on the dislocation length. However, we have found that the behavior of screw dislocation motion in the Ni-Fe alloy depends strongly on the dislocation length. We, therefore, studied this effect, modeling dislocation segments of different lengths from L_D = 4|***b***| (~0.99 nm) to 284|***b***| (~70 nm).

The mobility of a screw dislocation in the Ni-Fe alloy was found to depend on many factors, including both environmental and modelling effects. The environmental factors of applied stress, strain rate and temperature are similar to those affecting mobility of dislocations in pure Ni. Figure 2 presents the observed glide distance vs. time of a medium length dislocation segment (L_D =64|b|) for 100, 150 and 200 MPa applied shear stresses at different temperatures. In general, one can see that at 100 MPa the

dislocation moves in a very discontinous manner, being stuck at some positions for a quite long time. At this stress level, only at the highest T=900 K does the dislocation exhibit long-range motion. At all other temperatures, the dislocation moves to a favourable position where it remains immobilised at least for the modelled time, ~50 ns. At 150 MPa, Fig. 2b, the dislocation can move at ≥700 K, keeping the same characteristics, e.g., it is frozen for a while in some configurations. However, as seen in Fig. 2c, at 200MPa, the dislocation glides continuously, and the glide distance versus time dependence is linear at all temperatures studied here and close to that of pure Ni at 300K (dashed blue line).

For "low" stress deformation, corresponding to strain rates in the range $\dot{\varepsilon}$ =10^5–10^6 s^{-1}, the flow stress in pure Ni depends strongly on the temperature and decreases down to a few MPa at >100K. An example of dislocation velocity, V_D, versus applies shear stress, τ, is shown in Fig. 3a for 300K and 900K. The dependence is quite linear on the log-log plot which implies a practically constant dislocation friction coefficient, *B*, defined by:

$$v_D = \frac{\tau b}{B} \#(3)$$

and shown in Fig.3b. There are different mechanisms for friction in dislocation motion [10]; however, in most MD modelling, friction in elemental systems is controlled mainly by phonon damping.

A comparison of velocity-stress behaviour in pure Ni and the Ni-Fe alloy is shown in Fig. 3a. The behaviour of this dependence in the alloy at stresses below 200 MPa indicates a strong stress dependence of the friction coefficient. Indeed, this can be seen in Fig. 3b where the friction coefficient is presented as function of applied stress. In pure Ni, the drag coefficient *B* is nearly independent of stress and temperature. In contrast, for the Ni-Fe alloy at T=300 K, the value of *B* decreases from ~58 MPa·s to ~0.43 MPa·s when the applied stress increases from 100 MPa to 400 MPa, while at 900K, *B* drops from ~1.5 MPa·s down to ~0.49 MPa·s over the same stress range. Above a stress of 200 MPa, the behaviour

of Ni and NiFe are essentially identical. This provides evidence of a stress-dependent transition from pinned to unpinned behaviour.

Modelling factors affecting the behavior, i.e., those which are specific for the particular modelling case, are: (a) a particular spatial distribution of Ni and Fe for the alloy, and (b) the dislocation length, L_D. These factors are important for the equiatomic alloy (and for concentrated alloys in general), but less significant for dilute alloys and are not important at all for pure materials.

The importance of a particular spatial distribution of alloy components can be recognized, for example, in Fig. 2a (red line), where at 900K and τ=100 MPA, the dislocation was delayed several times including quite a long time (>10 ns) at ~330 nm. This means that the distribution of alloy components along the dislocation line acted as a relatively strong "obstacle" at a glide distance of ~330 nm from the initial position, and the dislocation needed ~17 ns time to overcome this at 900 K, whereas at 500 K and 700 K it was stuck there over the whole modelling time. The same "obstacle" was not bypassed at 500 K and 700 K for at least ~50 ns. Interestingly, at higher stress, τ=150 MPa, the dislocation could overcome this "obstacle" at 700 K but not at 500 K. At a lower temperature, 300 K, the dislocation was completely immobilized at distance ~7 nm from the initial position. This "obstacle" was seen by the dislocation at T=500K but did not pose a significant barrier at higher temperatures (see Fig. 2a). We note that these obstacles clearly dominate the behavior, yet they are very different from models of individual "solute" particles given that disorder in the present case means that the dislocation samples a large number of both atom types at every position.

These "obstacles" appear to be localized since the flow stress depends on the length of the gliding dislocation segment. The effect of the dislocation line length can be seen in Fig. 4, where the motion of medium (64|**b**|) and long (142|**b**|) dislocations are compared at different applied stresses and temperatures. The overall conclusion is that longer dislocations glide for longer distances at the same applied stress.

However, even the long dislocation encounters an impenetrable obstacle for 150 MPa at 300 K (dark cyan line). At higher temperature and stress, long-distance glide was observed for the long dislocation. It is important to note here that a conclusion about dislocation mobility can be made only by analyzing its long-range movement when the dislocations passes through many different states. Thus, in Fig. 4, one can see that a long dislocation at an applied stress of 150 MPa at 300K moved more than 600 nm before it found an "obstacle" able to stop it. Thus, one can conclude that this dislocation is not mobile although it still may overcome the obstacle by thermal activation as can be observed for other cases presented in Fig.4.

As mentioned in section 2, stress-controlled conditions for dislocation motion do not allow for an accurate estimation of the flow stress. For example, the results for $t<10$ ns at 500 K in Fig. 4 would suggest different distances of flow for the different lengths, and that a shear stress of 100 MPa is nearly sufficient to produce regular motion of the dislocation. However, neither simulation result at this temperature is representative of the longer time results, which show long residence times for dislocations at particular positions. We therefore applied strain-control to estimate the flow stress and its temperature and dislocation line-length effects. Figure 5 presents the evolution of shear stress generated during dislocation glide under applied shear strain. Two effects were tested: strain rate (Fig. 5a) and dislocation segment length (Fig. 5b). In both cases, the stress-strain dependence is a saw-tooth shaped combination of local maxima and minima with the stress growing linearly to a maximum and then dropping, sometimes even to a negative value. Within the investigated range, the deformation rate $\dot{\varepsilon}$ (or equivalently the average dislocation speed) weakly affects the stress-deformation behaviour, although some features can be observed. For slow dislocation velocities, most of the stress maxima and stress minima are lower (compare black, red and blue maxima in Fig. 5a).

The saw-tooth shaped stress-deformation dependences shown in Fig. 5 represent combinations of linear increases (primarily elastic deformation) and sudden drops (dislocation motion) and are qualitatively similar to those observed for dislocation glide through a population of obstacles in FCC materials (see, e.g., [21]). Indeed, the distribution of alloying components is random and not uniform locally. Fluctuations in the local composition locally affect the dislocation energy and thus can act as pinning "obstacles". In this case, the stress fluctuations should depend on the dislocation line length and be larger for short dislocations and smaller for long dislocation where they are averaged over the dislocation length. We have studied and shown this in a series of targeted simulations examining the role of dislocation length. The results obtained at 300 K and $\dot{\varepsilon}=10^6$ s^{-1} for dislocations of different length are presented in Fig. 5b. One can see that the shortest simulated dislocation segment, $L_D=4|\boldsymbol{b}|$ (black line), demonstrates the largest fluctuations in the shear stress, while the longest one, $L_D=142|\boldsymbol{b}|$ (red line), has the smallest fluctuations. Thus, long dislocation lines become more self-averaging, and also present lower barriers to dislocation motion.

Usually, localized obstacles produce a dependence of the critical resolved shear stress (CRSS) that is inversely proportional to the dislocation segment length, i.e., $1/L_D$. Results obtained for dislocations of different lengths modelled in different crystals, i.e., different random distributions of the alloying components, are summarized in Fig. 6, where the average maximum and mean stresses were evaluated during dislocation glide (T=300K and $\dot{\varepsilon}=10^6$ s^{-1}). The maximum stress, τ_{max}, was identified using a simple procedure. Five different random equiatomic Fe-Ni alloys were prepared, and the dislocation motion in these was examined over a few tens of nm at the same temperature and strain rate. Maximum values of the stress generated in each individual simulation were then averaged to produce the final value. For example, for the short dislocation presented in Fig. 5b (black line), $\tau_{max} \approx 460$ MPa. (Note that only a part of the whole stress-deformation dependence is presented in Fig. 5b). The standard deviation of this

value is 38 MPa, estimated by applying the technique described in [30] to pure Ni at 300K and a strain rate $\dot{\varepsilon}$=10^6 s^{-1}. The mean shear stress, $\bar{\tau}$, shown in Fig. 6, was estimated as the mean stress during a strain-rate controlled simulation (similar to that presented in Fig. 5b) averaged over all simulations. In general, the flow stress decreases with increasing L_D and saturates above ≈140|***b***|: $\bar{\tau}$ at ~40 MPa, while τ_{max} saturates at ~130 MPa.

The limited length of the simulated trajectory produces different accuracies in estimating $\bar{\tau}$ and τ_{max}. The mean stress has better statistical behavior and saturates faster. The maximum stress is related to a *local compositional configuration that produces the maximum high strength.* The probability of this configuration being encountered (and thus the values of τ_{max}) increases with increasing the total dislocation glide distance, i.e., the length of stress-deformation dependencies shown in Fig. 5b. Therefore, the shear stress shown in Fig. 6 as τ_{max} is a lower-bound value estimation of the maximum stress, i.e., the *flow stress*.

Given that the results suggest strong, localized pinning sites, it is natural to examine the structure of the dissociated dislocations for evidence of localized pinning. A visual analysis of the dislocation structure during its motion showed that the structure, e.g., the distance between two partial dislocations, changes along the line and glide path, that is, the longer is the dislocation line and glide path the more variable its configuration. An example is presented in Fig. 7 which shows a few instant configurations of the stacking fault ribbon of the longest dislocation, L_D = 142|b|, simulated at 300K together with the stacking fault ribbon observed in pure Ni under the same conditions. Several important features can be seen in Fig. 7 such as a wider dislocation dissociation in the alloy (indicating a lower stacking fault energy) and a non-uniform shape of the stacking fault ribbon in the alloy, indicating the strong local fluctuations of the dislocation line properties and stacking fault energy. No strong evidence of significant bowing of a dislocation under stress, which would indicate strong local pinning, is observed.

4. Discussion

We have used molecular dynamics simulations to study the mobility of ½<110> screw dislocations in equiatomic FCC Ni-Fe alloys and have found that dislocation velocity depends strongly on the applied stress, dislocation segment length and temperature. For a random solid solution of a NiFe alloy, there is a clearly defined threshold stress above which dislocations can glide. This stress was defined as a maximum stress over a long dislocation moving under strain-controlled simulation conditions. The simulation techniques used here allow the dislocations to undergo quite long-distance glide, ~10^2-10^3 nm, providing a high accuracy in estimating the maximum stress. Application of stress-controlled conditions for dislocation motion results in a similar stress value. This threshold stress is, in fact, the flow stress, τ_F, which depends on the dislocation segment length, L_D, and temperature, T. The flow stress tends to saturate at a value of $\tau_F \approx 130$ MPa either at $L_D \approx 140|\mathbf{b}|$ (T=300 K) and also at temperatures above $T \approx 500$ K (L_D=64|**b**|), as shown in Fig. 6. This high stress demonstrates that the NiFe alloy exhibits quite significant strengthening in comparison with pure Ni, where a screw dislocation at T=300 K glides smoothly at stresses as low as 5 MPa (see Fig. 1). This is in agreement with the argument of [18], which states that the Peierls stresses are negligible. In our simulations, for pure Ni, only the Peierl's barrier exists, and dislocation flow is easy, whereas for NiFe, there are strong barriers to motion. For stresses above τ_F, Ni and NiFe behave similarly, presumably as the stress reduces the barriers to ~k_BT or below; below τ_F, NiFe behaves quite differently. Thus, we observe two modes of motion in NiFe, in contrast to Ni.

There are very few published experimental studies of Ni-Fe binary alloys, but in one recent study, recovery, crystallization grain growth and phase stabilty of a family of FCC multicomponent equiatomic solid solutions, including Ni-Fe, were examined [31]. Temperature effects on mechanical properies were

compared for Ni and Ni-Fe equiatomic alloy in [32]. It was found that at room T, the yield stress in pure Ni is ~100 MPa while in the Ni-Fe alloy it is equal to ~180 MPa. The ultimate tensile strength was found to be ~340 MPa in Ni and ~500 MPa in NiFe. The difference between Ni and NiFe is ~80-160 MPa which compares reasonable well with the ~130 MPa flow stress obtained here for the longest dislocation line. Temperature activated mechanisms and Labusch strengthening were analysed for different equiatomic solid solutions in [33].

The two-mode motion of a screw dislocation in the equiatomic Ni-Fe alloy observed here is important for understanding the temperature dependence of the dislocation velocity. If the applied stress in the Ni-Fe alloy is below τ_F, the dislocation moves in a very discontinuous way, and its motion is controlled by thermal activation processes over different local "obstacles" and is therefore strongly temperature dependent. These obstacles vary in strength, and their behavior is likely governed by rare, strong obstacles to motion. This is evident in Fig. 2, where the dislocation under 100 MPa of shear stress and at temperatures > 300 K, encounters strong pinning at a position ~330 nm from its initial position. The pinning is sufficiently strong that at this stress level that the dislocation does not escape for the rest of the simulation at T=500 K and 700 K, and also remains at that position for a long period at T=900 K. This same position is evident at stress levels of 150 MPa (Fig. 2b), although the thermal activation to escape from this location is clearly easier. For a long dislocation traveling 300 nm, many local configurations are sampled, suggesting that the strongly pinned dislocation location is not dependent on a particular local configuration along the dislocation line. On the other hand, the result that τ_F depends on L_D is evidence that these "obstacles" are somehow localized. An alternate view is that the statistics of the behavior along the line is what dominates, and a sufficient length L_D is required to become self-averaging. The fact that τ_F saturates at $L_D \approx 140|\mathbf{b}|$ gives an upper estimation of the concentration of these "obstacles."

If the applied stress is above τ_F, the dislocation glides freely with high velocity, and the temperature dependence is rather weak above 300-500K, as follows from Fig. 6.

Interestingly, the two-mode dislocation motion can be predicted on the basis of a solute strengthening model developed in [18, 19] for concentrated solid solution alloys. In this model, it is assumed that a dislocation glides over a field of obstacles distributed in the averaged matrix media. The obstacles are assumed to arise from local composition fluctuations and are treated as objects with a certain misfit volume, elastic properties, size and distance between them. Parameters characterizing edge dislocation-obstacle interactions depend on the particular alloy, and examples of parameterization for some Ni-based multicomponent alloys are described in [19]. The two-mode dislocation motion observed here for a screw dislocation is qualiatatively consistent with this theory. A more precise comparison with this solute strengthening model [19] was not a specific aim of the present study, but we have made efforts to clarify the nature of internal obstacles for dislocation glide. However, analysis of the local atomic structure of a moving dislocation did not result in any simple conclusions or structural explanations. Fig. 7 shows the dissociated dislocation for pure Ni, along with several configurations taken during the constant strain-rate simulations. The width of the stacking fault ribbon and, therefore, the dissociation distance between Shockley partial dislocations observed in the alloy, is much wider than in pure Ni. This is consistent with a general decrease of stacking fault energy observed in Ni-Fe alloys [34]. However, there is also a significant variation in the dissociation distance along the line of long dislocation. The variation in position along the line, shown in Fig. 7, appear to be similar to that shown in Fig. 3 of [19]. This is evidence that the local dissociation conditions, likely to be composition dependent, vary significantly. However, the dislocation line does not curve significantly, demonstrating that the "obstacles" are not so strong to cause a significant curvature, at least for line lengths considered here. This appears to be similar to the argument presented in [18]: static structures appear to be vary along the line length, to minimize

energy, without significant bowing. Therefore, the quite high peaks in the stress during dislocation motion (see Fig. 5) are not purely associated with localized obstacles. At low temperatures, Fig. 6 shows a mean stress during strain-controlled simulations near 200 MPa, and a maximum stress near 400 MPa. This is roughly in agreement with the molecular statics results of [18] in the low-Cr limit, though the methods and potentials are different. In particular, the simulations of [18] use molecular statics (i.e. at $T=0$ K), with many simulations of dislocation motion over distances of ~1 nm, whereas the work presented here shows results over tens and hundreds of nm at a range of temperatures, under both stress- and strain-controlled simulations.

In summary, our results show that the dislocation behavior in equiatomic FCC NiFe exhibits two modes of behavior: an obstacle-dominated regime at low stresses, and a smooth behavior similar to pure Ni at high stresses (>150 MPa). In contrast, pure Ni shows smooth glide behavior for all stresses above 5 MPa. In the high stress regime, the dislocation velocity and drag coefficient for NiFe are close to those of Ni, with little temperature dependence (see Fig. 3). In the lower stress regime, NiFe has a much higher drag coefficient and lower dislocation velocity than pure Ni, and these properties are clearly temperature dependent. The behavior is dominated by local configurations that strongly pin the dislocation. These local configurations are not sharply localized along the dislocation line, but exhibit a mixture of local and delocalized behavior. We hypothesize that this is dependent on the statistics of local configurations and compositions along the dislocation line, and will explore these in a subsequent work.

Acknowledgements: This work was supported by the U. S. Department of Energy's Office of Science, Basic Energy Sciences, Materials Science and Engineering Division.

Copyright notice: *This manuscript has been authored by UT-Battelle, LLC under Contract No. DE-AC05-00OR22725 with the U.S. Department of Energy. The United States Government retains and the publisher, by accepting the article for publication, acknowledges that the United States Government retains a non-exclusive, paid-up, irrevocable, world-wide license to publish or reproduce the published form of this manuscript, or allow others to do so, for United States Government purposes. The Department of Energy will provide public access to these results of federally sponsored research in accordance with the DOE Public Access Plan (http://energy.gov/downloads/doe-public-access-plan).*

References

1. B. Cantor, I.T.H. Chang, P. Knight, A.J.B. Vincent, Microstructural development in equiatomic multicomponent alloys, Mater. Sci. Eng. A, 375 (2004) 213.
2. F. Otto, Y. Yang, H. Bei, E.P. George, Relative effects of enthalpy and entropy on the phase stability of equiatomic high-entropy alloys, Acta Mater., 61 (2013) 2628.
3. Z. Wu, H. Bei, F. Otto, G.M. Pharr, E.P. George, Recovery, recrystallization, grain growth, and phase stability of a family of FCC-structured multi-component equiatomic solid solution alloys, Intermetallics, 46 (2014) 131.
4. R. Kozak, A. Sologubenko, W. Steurer, Single-phase high-entropy alloys - an overview, Z. Kristallogr., 230 (2015) 55.
5. J.W. Yeh, S.K. Chen, S.J. Lin, J.Y. Gan, T.S. Chin, T.T. Shun, C.H. Tsau, S.Y. Chang, Nanostructured high-entropy alloys with multiple principle elements: Novel alloy design concepts and outcomes, Adv. Eng. Mater., 2004, 6, 299.
6. X. Yang, Y. Zhang, Prediction of high-entropy stabilized solid-solution in multi-component alloys, Mater. Chem. and Phys., 132 (2012) 233.
7. M.C. Troparevsky, J.R. Morris, P.R.C. Kent, A.R. Lupini, G.M. Stocks, Criteria for Predicting the Formation of Single-Phase High-Entropy Alloys, Phys. Rev., X., 5 (2015) 011041.
8. O.N. Senkov, G.B. Wilks, J.M. Scott, D.B. Miracle, Mechanical properties of Nb25Mo25Ta25W25 and V20Nb20Mo20Ta20W20 refractory high entropy alloys, Intermetallics, 2011, 19, 698.
9. Z. Wu, H. Bei, G.M. Pharr, E.P. George, Temperature dependence of the mechanical properties of equiatomic solid solution alloys with face-centered cubic crystal structures, Acta Mater., 81 (2014) 428.

10. S.G. Ma, S.F. Zhang, J.W. Qiao, Z.H. Wang, M.C. Gao, Z.M. Jiao, H.J. Yang, Y. Zhang, Superior high tensile elongation of a single-crystal CoCrFeNiAl0.3 high-entropy alloy by Bridgman solidification, Intermetallics, 54 (2014) 104.
11. B. Gludovatz, A. Hohenwarter, D. Catoor, E.H. Chang, E.P. George, R.O. Ritchie, A fracture-resistant high-entropy alloy for cryogenic applications, Science, 345 (2014) 1153.
12. B. Gludovatz, A. Hohenwarter, K.V.S. Thurston, H. Bei, Z. Wu, E.P. George, R.O. Ritchie, Exceptional damage tolerance of a medium-entropy alloy CrCoNi at cryogenic temperatures, Nature Comm., 7 (2016) 10602.
13. F. Otto, A. Dlouhý, C. Somsen, H. Bei, G. Eggeler, E.P. George, The influences of temperature and microstructure on the tensile properties of a CoCrFeMnNi high-entropy alloy, Acta Mater., 61 (2013) 5743.
14. Z. Zhang, M.M. Mao, J. Wang, B. Gludovatz, Z. Zhang, S.X. Mao, E.P. George, Q. Yu, R.O. Ritchie, Nanoscale origins of damage tolerance of the high-entropy alloy CrMnFeCoNi, Nature Comm., 6 (2015) 10143.
15. W. Cai, V.V. Bulatov, J. Chang, J. Li, S. Yip, Dislocation Core Effects on Mobility, in "Dislocations In Solids vol. 12", edited by FRN Nabarro and JP Hirth, Elsevier (Amsterdam), 2004, p. 11.
16. R. Peierls, The size of a dislocation, Proc. Phys. Soc., 52 (1940) 34.
17. F.R.N. Nabarro, The Peierls stress for a wide dislocation, Mater. Sci. Eng., A 113 (1989) 315.
18. C. Varvenne, A. Luque, W.A. Curtin, Theory of strengthening in fcc high entropy alloys, Acta Mat., 118 (2016) 164.
19. C. Varvenne, G. Leyson, M. Ghazisaelidi, W.A. Curtin, Solute strengthening in random alloys, Acta Mat., 124 (2017) 660.

20. C. Varvenne, A. Luque, W.G. Nohring, W.A. Curtin, Average-atom interatomic potential for random alloys, Phys. Rev. B, 93 (2016) 104201.
21. T.M. Smith, M.S. Hooshmand, S.D. Esser, F. Otto, D.W. McComb, E.P. George, M. Ghazisaeidi, M. J. Mills,Atomic-scale characterization and modeling of 60 degrees dislocations in a high-entropy alloy, Acta Mat., 110 (2016) 352-363
22. S.I. Rao, C. Varvenne, C. Woodward, T.A. Parthasarathy, D. Miracle, O.N. Senkov, W.A. Curtin, Atomistic simulations of dislocations in a model BCC multicomponent concentrated solid solution alloy, Acta Mat. 125 (2017) 311-320
23. S.I. Rao, C. Woodward, T.A. Parthasarathy, O. Senkov, Atomistic simulations of dislocation behavior in a model FCC multicomponent concentrated solid solution alloy, Acta Mat. 134 (2017) 188-194.
24. S. Zhao, Y. Osetsky and Y. Zhang, Atomic-scale dynamics of edge dislocations in Ni and concentrated solid solution NiFe alloys, Journal of Alloys and Compounds, 701 (2017) 1003-1008.
25. Yu.N.Osetsky and D.J.Bacon, An atomic-level model for studying the dynamics of edge dislocations in metals. Modelling Simul.Mat.Sci.Eng.,11 (2003) 427.
26. J.Bacon, Yu.N.Osetsky and D.Rodney, Dislocation-Obstacle Interactions at the Atomic Level, 2009,Chapter 88, Series : "Dislocations in Solids", Ed. by J.P.Hirth and L.Kubin, (ISBN: 978-0-444-53285-5; ISSN: 1572-4859), pg.1-90.
27. D Rodney, Molecular dynamics simulation of screw dislocations interacting with interstitial frank loops in a model FCC crystal, Acta Materialia 52 (2004) 607.
28. H.J.C. Berendsen, J.P.M. Postma, W.F. van Gunsterne, A. DiNola, J.R.Haak, Molecular dynamics with coupling to an external bath, J. of Chem. Phys., 81 (1984) 3684.
29. G.Bonny, D.Terentyev, et al., Interatomic potential to study plasticity in stainless steels: the FeNiCr model alloy, Modelling Simul.Mat.Sci.Eng., 19 (2011) 085008.

30. Y.N. Osetsky and R.E. Stoller, Atomic-scale Mechanisms of Helium Bubble Hardening in Iron, *J. of Nucl. Mater.,* 465 (2015) 448-454.

31. Z. Wu, H. Bei, F. Otto, G.M. Pharr and E.P. George, Recovery, recrystallization, grain growth and phase stability of a family of FCC-structured multi-component equiatomic solid solution alloys, Intermetallics 46 (2014) 131-140.

32. Z. Wu, H. Bei, G.M. Pharr, E.P. George, Temperature dependence of the mechanical properties of equiatomic solid solution alloys with face-centered cubic crystal structures, Acta Mat. 81 (2014) 428–441.

33. Z. Wu, Y. Gao, H. Bei, Thermal activation mechanisms and Labusch-type strengthening analysis for a family of high-entropy and equiatomic solid-solution alloys, Acta Mat. 120 (2016) 108–119.

34. S. Zhao, Y.N. Osetsky, G.M. Stocks, Y.Zhang, Distribution of stacking fault energies in chemically complex concentrated solid-solution alloys, (2018), submitted.

Figures.

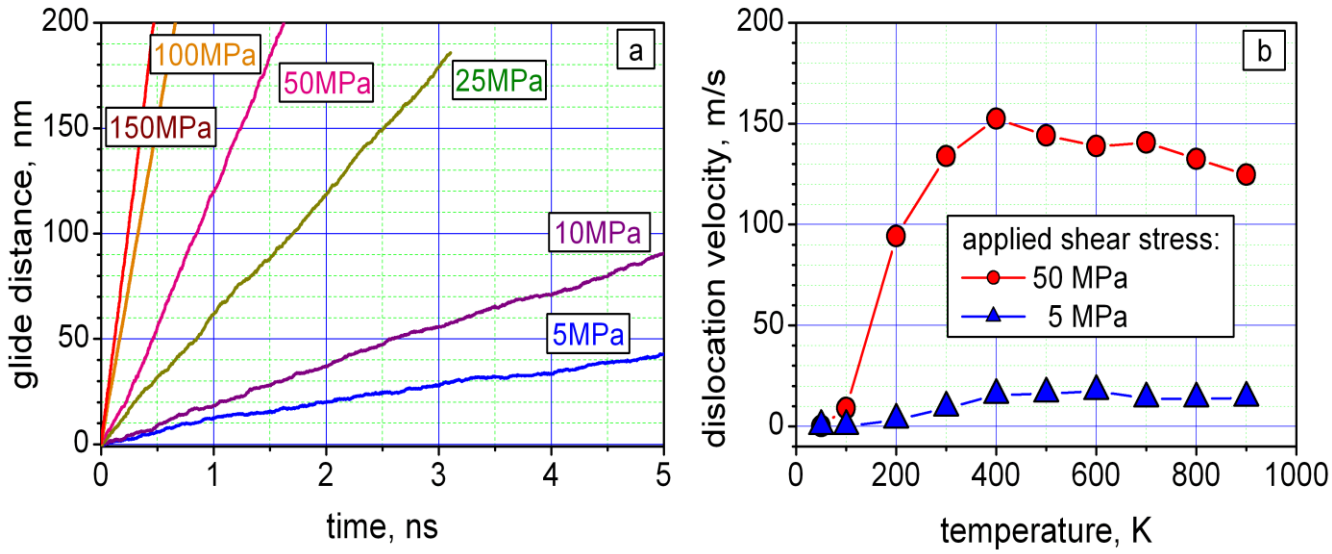

Figure 1. Dislocation glide in pure Ni exhibits smooth glide at the stresses and temperatures examined:

a) glide distance as function of time at 300K for applied shear stresses from 5 to 150 MPa;

b) temperature dependence of the dislocation velocity at 5 and 50 MPa applied shear stresses.

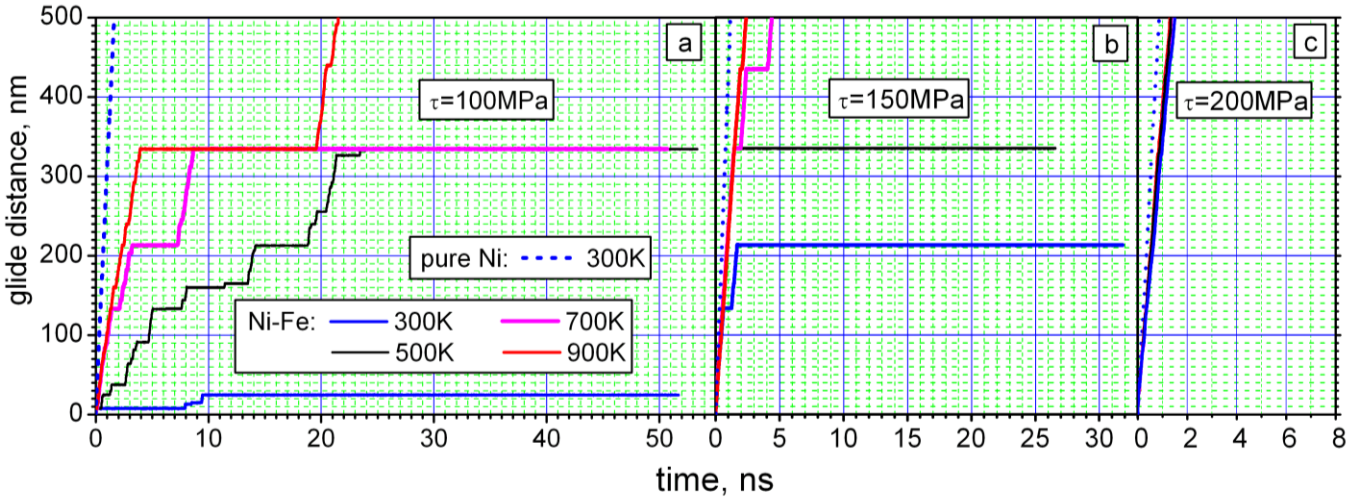

Figure 2. Dislocation glide for equiatomic Ni-Fe alloy shows discontinuous behaviour for applied stresses below 200 MPa (L_D =64|b|): Glide distance as function of time:

a) =100MPa; b) τ=150MPa; c) τ=200MPa.

Solid lines of different colour show Ni-Fe alloy at different temperatures. The dashed blue line is for pure Ni at 300K.

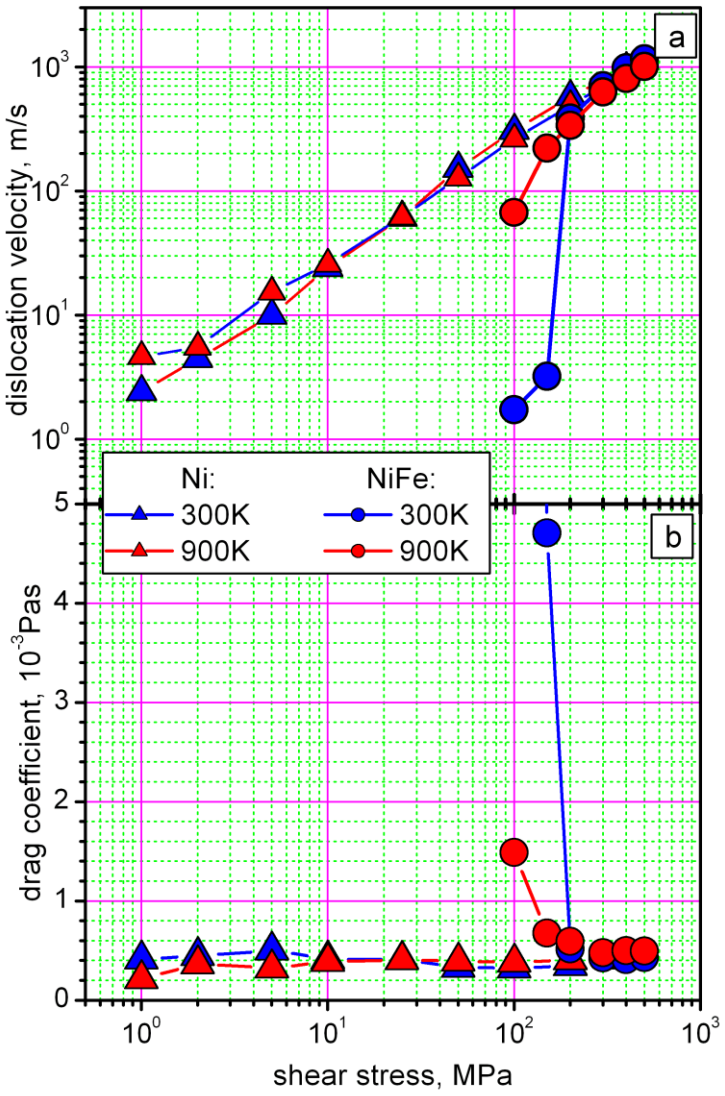

Figure 3. Dislocation glide parameters in Ni and in the equiatomic Ni-Fe solid solution (L_D =64|b|): (a) glide velocity and b) drag coefficient as function of applied shear stress at 300 and 900K.

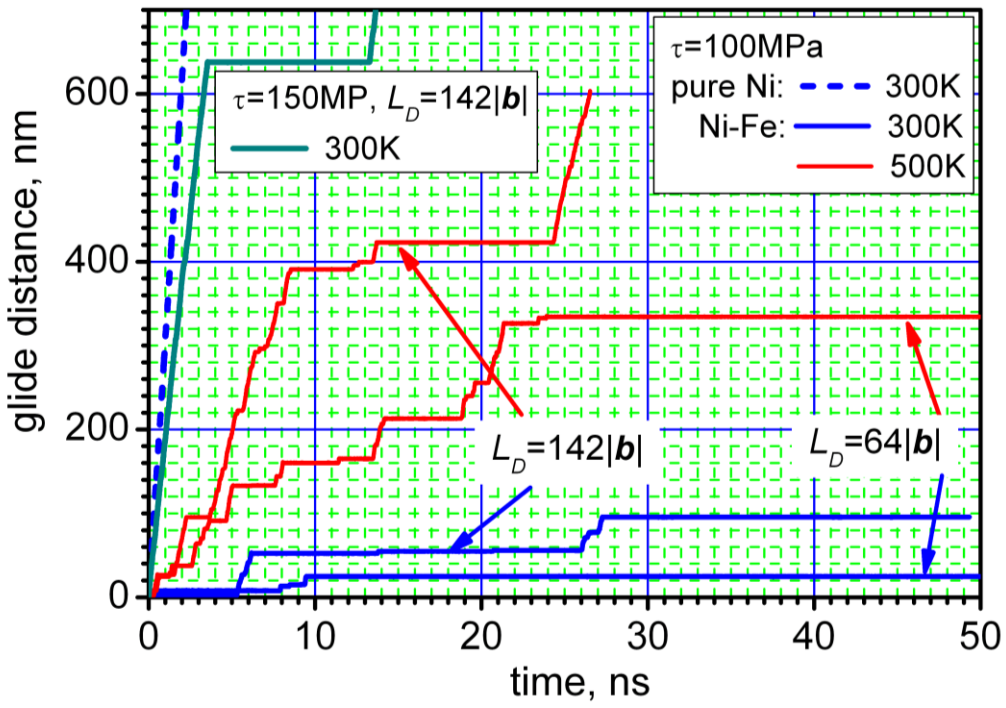

Figure 4. Dislocation glide distance versus time at applied shear stress:

- 100 MPa in pure Ni at 300K (blue dash line);
- 100 MPa medium (L_D =64|**b**|) and long (L_D =142|**b**|) dislocations at 300K (blue lines);
- 100 MPa medium and long dislocations at 500K (black lines)
- 150 MPa long dislocation at 300K (dark cyan line).

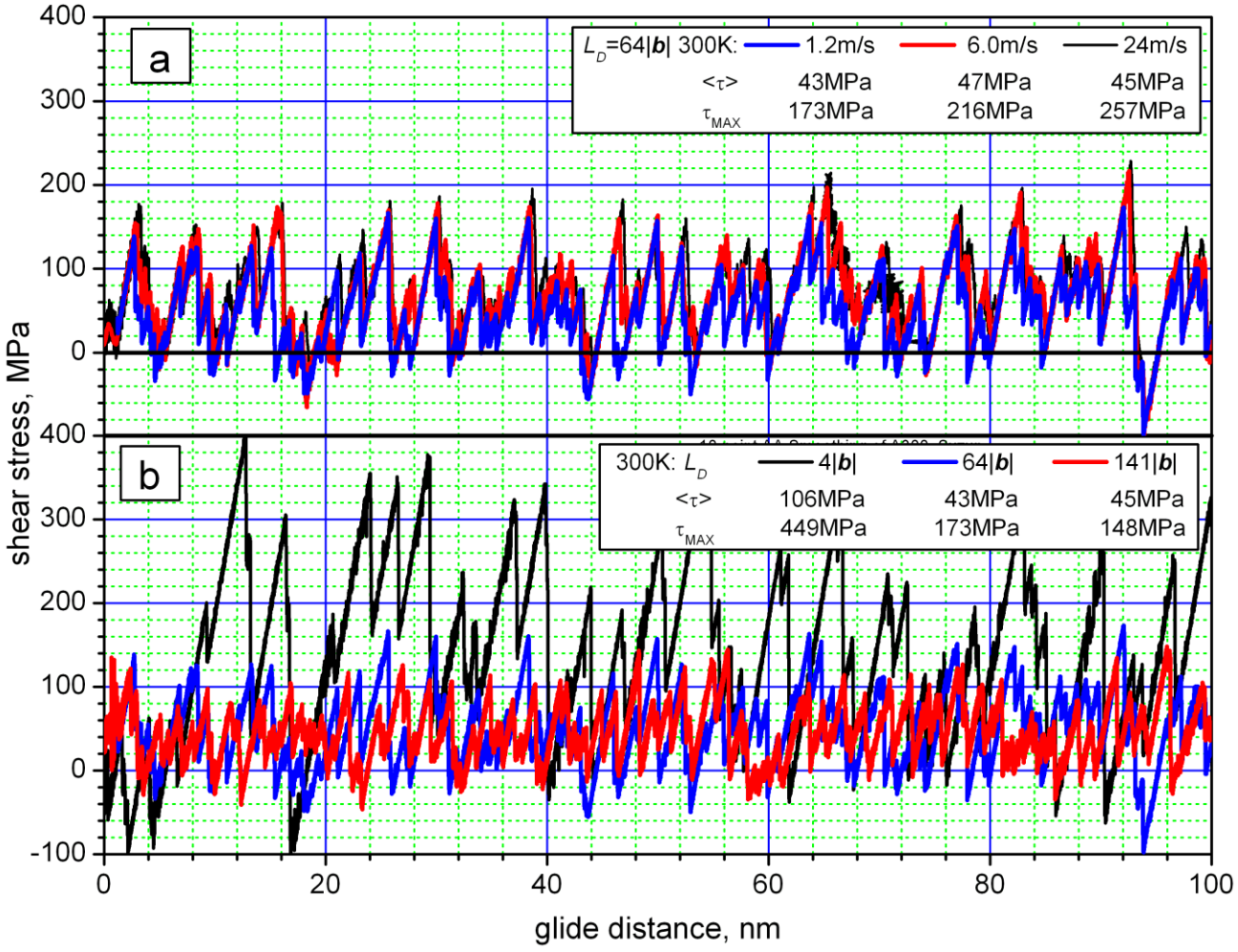

Figure 5. Dislocation glide for Ni-Fe under applied shear strain:

a) Shear stress vs glide distance for a dislocation with L_D=64|***b***| modelled at 300 K and at strain rates of 10^6 s^{-1}, $5x10^6$ s^{-1} and $2x10^7 s^{-1}$ that correspond to average velocities of 1.2, 6 and 24 m/s.

b) Shear stress vs glide distance for dislocations with L_D= 5|***b***|, 64|***b***| and 142|***b***| gliding at a strain rate of 10^6 s^{-1} (1.2 m/s) at 300 K.

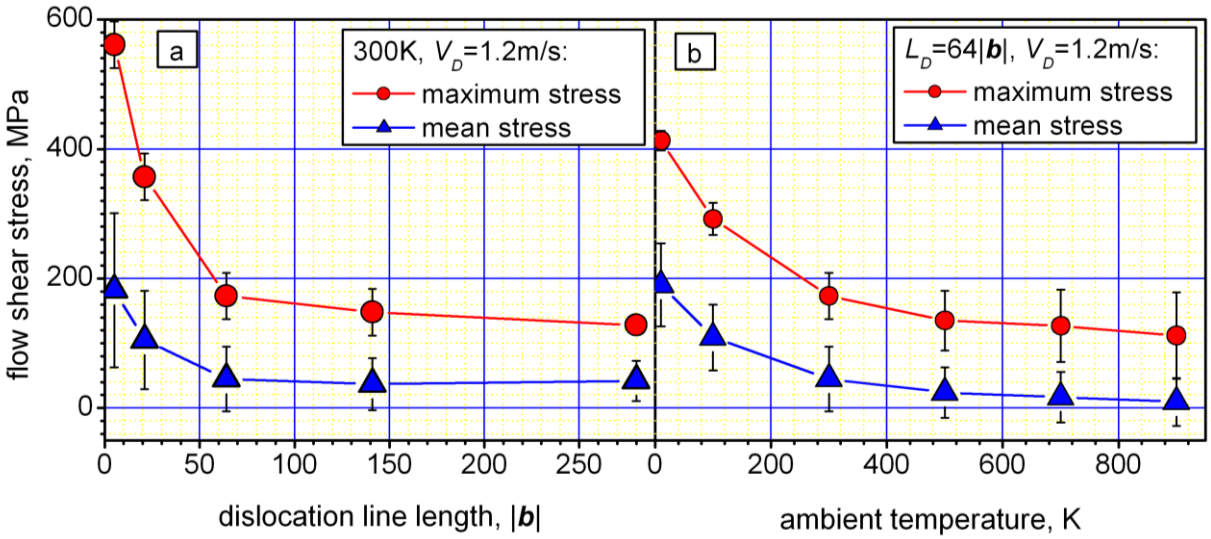

Figure 6. Dislocation glide of Ni-Fe under applied shear strain:

a) Mean and maximum stress as function of the dislocation line length.

b) Mean and maximum stress as function of temperature.

Error bars are standard deviations obtained by applying the technique described in [24] (for pure Ni at 300K and a strain rate $\dot{\varepsilon}=10^6$ s^{-1}) for the maximum stress and statistical treatment of all data (such as presented in Fig.5) for the mean stress.

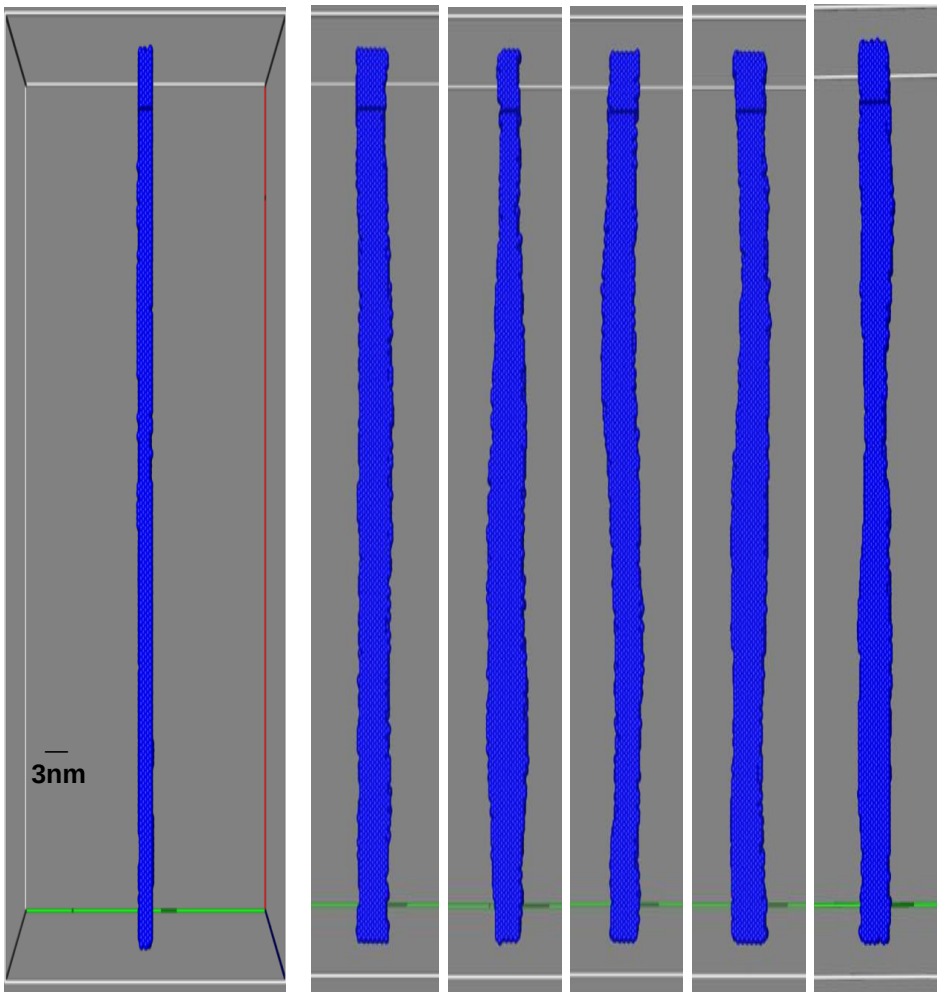

Fig. 7. Examples of stacking fault ribbon configurations obtained in modelling at 300K: Atoms belonging to the stacking fault ribbon of dislocation with L_D =142|***b***| moving at v_D = 1.2m/s in pure Ni (left image) and different instant configurations observed in the Ni-Fe alloy.

*Graphical Abstract

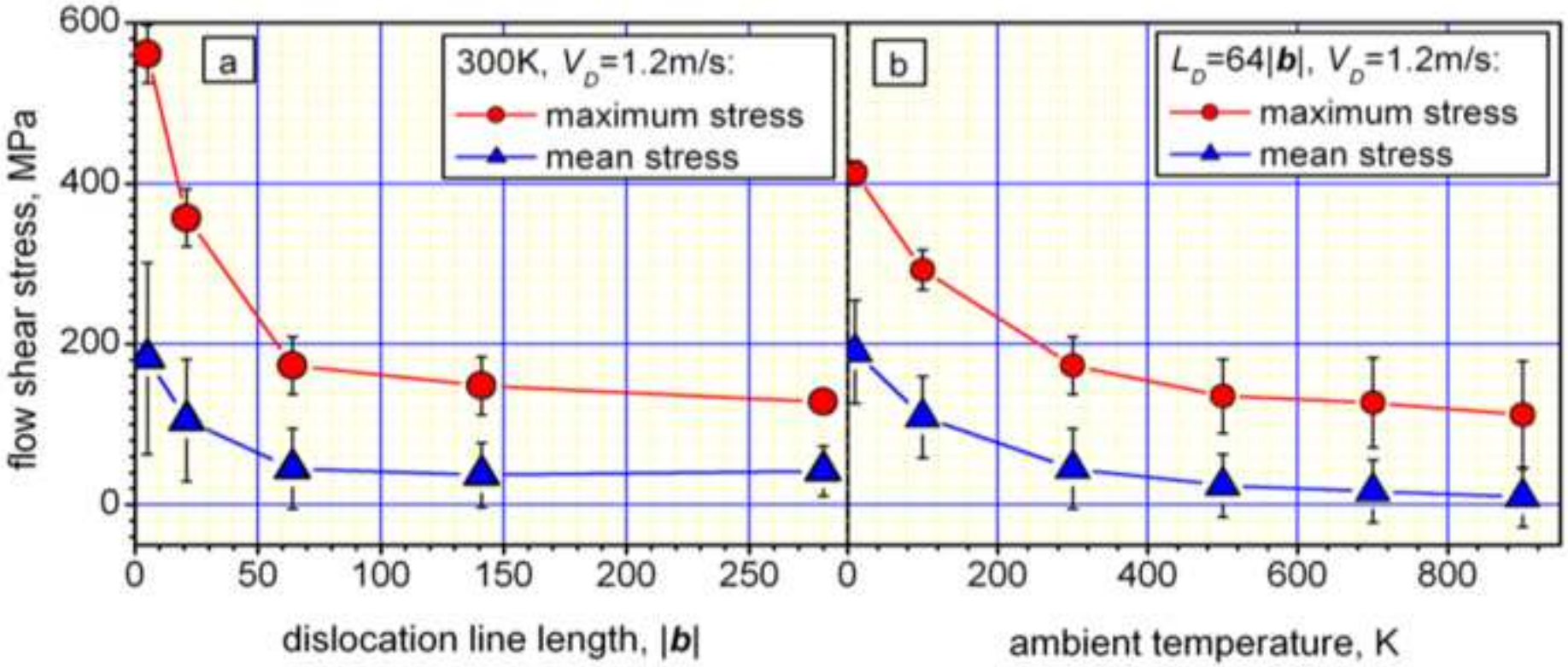

Dislocation glide of Ni-Fe under applied shear strain rate 10^6 s^{-1}